BULLETIN OF THE CHEMICAL SOCIETY OF JAPAN VOL. 42 372—378 (1969)

Optical and Acoustic Branches and Frequency Distribution of Polyethylene Glycol Chain

Hiroatsu MATSUURA and Tatsuo MIYAZAWA

Institute for Protein Research, Osaka University, Kita-ku, Osaka

(Received July 15, 1968)

Optical and acoustic branches of chain vibrations of polyethylene glycol were treated. The nature of these branches was elucidated on the basis of potential-energy distributions and phase relations. From dispersion curves (frequency *versus* phase difference), the frequency distribution of chain vibrations was calculated, in order to analyze thermal-neutron scattering spectra. Vibrational assignments of scattering peaks in the region 600—200 cm^{-1} were made with reference to the frequency distribution peaks and potential-energy distributions calculated for the single chain.

Infrared absorption, Raman scattering, and neutron inelastic scattering measurements are three important methods for studying chain vibrations of helical polymer molecules. The selection rules for infrared absorption and Raman effect are related with the angle (θ) of rotation, per unit, about the helix axis. Infrared absorption bands arise from vibrations with the phase difference of

$\delta=0$ or θ, while Raman lines arise from vibrations with $\delta=0$, θ, or 2θ.[1,2] For neutron scattering, however, there is no selection rule and chain vibrations for any phase difference contribute to inelastic scattering. Accordingly, frequency distribution peaks give rise to inelastic scattering peaks. For polyethylene glycol, neutron inelastic scattering was observed by Trevino and Boutin[3] and observed scattering peaks were analyzed with reference to the frequency distribution peaks calculated for an isolated chain of polyethylene glycol.[4]

In our previous study,[5] the force field of polyethylene-glycol chain was refined and the nature of observed infrared bands and Raman lines was discussed on the basis of potential-energy distributions. With the refined force field, in the present study, optical and acoustic branches of polyethylene-glycol chain were treated and the nature of these branches was elucidated. Dispersion curves (frequency *versus* phase difference) are useful for analyses of vibrational spectra of model oligomers in the crystalline state.[6] Also, the frequency distribution of chain vibrations was calculated and the nature of neutron scattering peaks was elucidated.

Normal Coordinate Treatment

Polyethylene-glycol chain is in the 7_2 helical conformation (seven units of CH_2CH_2O and two helical turns per fiber period),[7,8] having two twofold axes per unit. One axis bisects the C–O–C bond angle while the other axis intersects the C–C bond at right angle. Accordingly, this polymer chain belongs to dihedral group. A general method for treating helical chain vibrations was described previously.[2,9,10]

Normal vibrations of polyethylene-glycol chain were treated previously for the phase differences of $\delta=0$ (A_1 and A_2) and for $\delta=\theta$ (E_1).[5] In the present study, normal vibrations were treated for the phase differences of $\delta=0°$, 15°,⋯, 165° and 180°, with the interval of 15°.*1 Bond-stretching, angle-bending, and internal-rotation coordinates were transformed into local-symmetry coordinates; namely σ_{ss} (CH_2 symmetric stretching), σ_{as} (CH_2

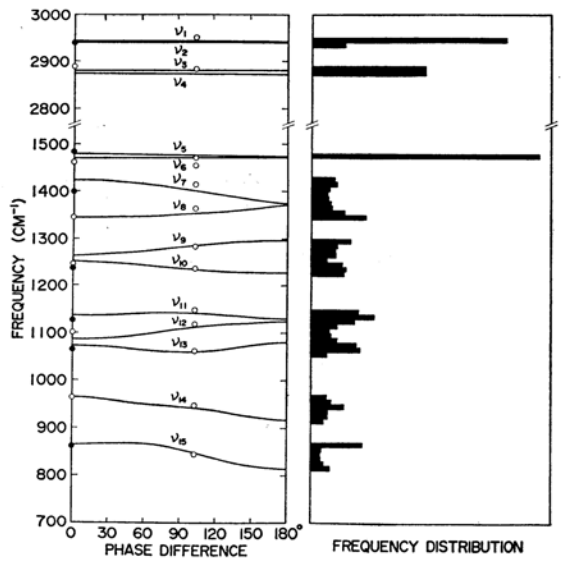

Fig. 1. Dispersion curves for the ν_1—ν_{15} branches and frequency distribution of polyethylene-glycol chain.
○: infrared absorption frequency
●: Raman frequency

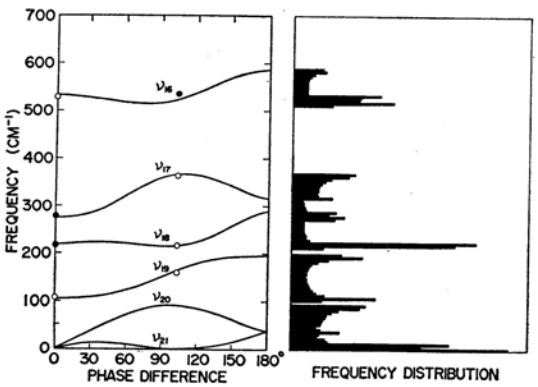

Fig. 2. Dispersion curves for the ν_{16}—ν_{21} branches and frequency distribution of polyethylene-glycol chain.
○: infrared absorption frequency
●: Raman frequency

*1 Only the phase-difference region of $0\leq\delta\leq\pi$ need be treated, since frequenices for $\delta=2\pi+\alpha$ are the same as for $\delta=\alpha$, and frequencies for $\delta=\pi+\beta$ are the same as for $\delta=\pi-\beta$.

1) P. Higgs, *Proc. Roy. Soc.* (*London*), **A220**, 472 (1953).
2) T. Miyazawa, *J. Chem. Phys.*, **35**, 693 (1961).
3) S. Trevino and H. Boutin, *J. Macromol. Sci.*, **A1**, 723 (1967).
4) H. Matsuura and T. Miyazawa, *Rept. Progr. Polymer Phys. Japan*, **9**, 179 (1966).
5) H. Matsuura and T. Miyazawa, This Bulletin, **41**, 1798 (1968).
6) H. Matsuura and T. Miyazawa, Symposium on Molecular Structure, Toyonaka, 1966; *Rept. Progr. Polymer Phys. Japan*, **10**, 187 (1967).
7) T. Miyazawa, *J. Polymer Sci.*, **55**, 215 (1961), addendum; T. Miyazawa, K. Fukushima and Y. Ideguchi, *J. Chem. Phys.*, **37**, 2764 (1962).
8) H. Tadokoro, Y. Chatani, T. Yoshihara, S. Tahara and S. Murahashi, *Makromol. Chem.*, **73**, 109 (1964); T. Yoshihara, H. Tadokoro and S. Murahashi, *J. Chem. Phys.*, **41**, 2902 (1964).
9) T. Miyazawa, *Nippon Kagaku Zasshi* (*J. Chem. Soc. Japan, Pure Chem. Sect.*), **88**, 111 (1967).
10) H. Sugeta and T. Miyazawa, *J. Chem. Phys.*, **47**, 2034 (1967).

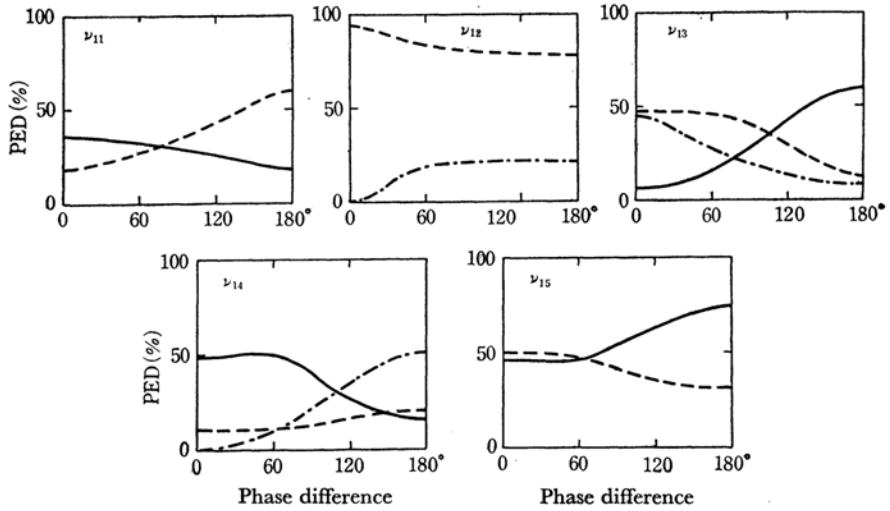

Fig. 3. Dependence of potential-energy distributions (PED) upon phase difference.
—— : σ_{ro}, ------ : $\sigma_{CO\ st}$, —·—·— : $\sigma_{CC\ st}$

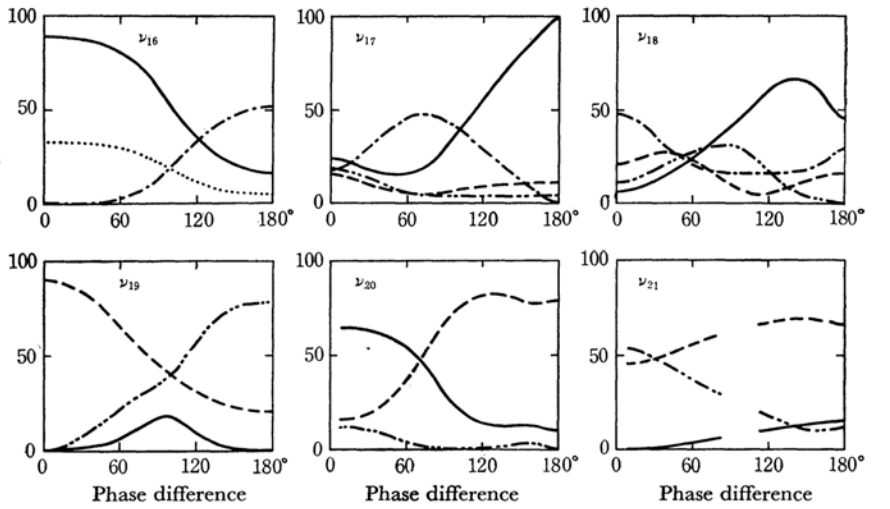

Fig. 4. Dependence of potential-energy distributions (PED) upon phase difference.
····· : σ_{ro}, —— : σ_{CCO}, —·—·— : σ_{COC}, —··—··— : $\sigma_{CC\ to}$, ---- : $\sigma_{CO\ to}$

antisymmetric stretching), σ_{sc} (CH_2 scissoring), σ_{wa} (CH_2 wagging), σ_{tw} (CH_2 twisting), σ_{ro} (CH_2 rocking), $\sigma_{CC\ st}$ (C–C stretching), $\sigma_{CO\ st}$ (C–O stretching), σ_{CCO} (C–C–O bending), σ_{COC} (C–O–C bending), $\sigma_{CC\ to}$ (C–C internal-rotation), and $\sigma_{CO\ to}$ (C–O internal-rotation).[5] Inverse-kinetic energy matrices $\boldsymbol{G}(\delta)$ were constructed with the molecular parameters listed previously.[5]

Local-symmetry force constants[11] of polyethylene-glycol chain were refined previously[5] so that frequencies calculated for A_1, A_2 and E_1 vibrations reproduce observed infrared and Raman frequencies with a root-mean-squared deviation as small as 0.9%. The same set of force constants was used in the present study for constructing potential-energy matrices $\boldsymbol{F}(\delta)$.

Vibrational frequencies calculated for $\delta=0°$, 60°, 120°, and 180° are listed*2 in Tables 1 and 2, together with potential-energy distributions (PED) and phase-angle differences[5,9] (phase relations in normal modes of degenerate vibrations). Vibrational modes with $\Delta\varepsilon(OCH_2\text{–}CH_2O) \sim 0°$ and $\sim \pm 180°$ are quasi-symmetric and quasi-antisymmetric, respectively, with respect to the twofold axis that intersects the CH_2–CH_2 bond. Similarly, vibrational modes with $\Delta\varepsilon$(C–O–C) $\sim 0°$ and $\sim \pm 180°$

11) T. Shimanouchi, *Nippon Kagaku Zasshi* (*J. Chem. Soc. Japan, Pure Chem. Sect.*), **86**, 261, 768 (1965); Symposium on Molecular Structure, Tokyo, 1964; Toyonaka, 1966.

*2 A more detailed list is given in Ref. 13, p. 69, including $\delta=30°$, 90° and 150°.

are quasi-symmetric and quasi-antisymmetric, respectively, with respect to the twofold axis that intersects the C–O–C angle. For the phase difference of $\delta=0°$, chain vibrations are classified into A_1 vibrations [$\Delta\varepsilon=0°$] and A_2 vibrations [$\Delta\varepsilon=180°$] while for the phase difference of $\delta=180°$, chain vibrations are classified into B_1 vibrations [$\Delta\varepsilon(OCH_2–CH_2O)=0°$ and $\Delta\varepsilon(C–O–C)=180°$] and B_2 vibrations [$\Delta\varepsilon(OCH_2–CH_2O)=180°$ and $\Delta\varepsilon(C–O–C)=0°$].

Dispersion curves (frequency *versus* phase difference) of twenty-one vibrational branches of polyethylene-glycol chain are shown in Figs. 1 and 2, together with observed infrared and Raman frequencies (excepting ν_{16}, only the infrared frequencies are shown for $\delta=\theta$). Main terms of potential-energy distributions for the branches ν_{11}—ν_{21} are shown in Figs. 3 and 4.

High Frequency Branches

For a helical polymer chain, two branches in the lowest-frequency region are acoustic branches, and other higher-frequency branches are optical branches. For polyethylene glycol, there are seven atoms per repeat unit of CH_2CH_2O, and accordingly chain vibrations consist of twenty-one branches, namely nineteen optical and two acoustic branches (Figs. 1 and 2).

In the highest-frequency region of 3000—2800 cm^{-1}, there are four branches, ν_1—ν_4. The ν_1 and ν_2 branches are associated with CH_2 antisymmetric stretching modes, while ν_3 and ν_4 branches are associated with CH_2 symmetric stretching modes (Table 1). With respect to the local twofold symmetry axis, the ν_1 and ν_3 branches are quasi-antisymmetric ($160°<\Delta\varepsilon\leq180°$) whereas the ν_2 and ν_4 branches are quasi-symmetric ($0°\leq\Delta\varepsilon<20°$). Atomic displacements of these vibrations are highly localized in the CH_2–CH_2 groups so that frequencies of these four branches do not vary with phase difference.

In the polarized infrared spectra of polyethylene glycol, the parallel band at 2890 cm^{-1} is assigned to the $\nu_3(0)$ vibration (A_2), the perpendicular band at 2950 cm^{-1} to the $\nu_1(\theta)$ and $\nu_2(\theta)$ vibrations (E_1), and the perpendicular band at 2885 cm^{-1} to the $\nu_3(\theta)$ vibration (E_1). The medium-intensity Raman line at 2939 cm^{-1} is assigned to the $\nu_2(0)$ vibration while the strong line at 2890 cm^{-1} is assigned to the CH_2 symmetric stretching modes (ν_3 and ν_4).

The ν_5 and ν_6 branches are associated with quasi-symmetric and quasi-antisymmetric scissoring modes, respectively, of CH_2–CH_2 groups (Table 1). Frequencies of these two branches vary little with phase difference. The doublet parallel bands at 1463 and 1457 cm^{-1} are assigned to $\nu_6(0)$ (A_2) and the perpendicular bands at 1470 and 1453 cm^{-1} are assigned to $\nu_5(\theta)$ and $\nu_6(\theta)$ (E_1), respectively. The strong Raman line at 1484 cm^{-1} is assigned to $\nu_5(0)$ (A_1) and weak line at 1449 cm^{-1} to $\nu_6(\theta)$.

TABLE 1. CALCULATED FREQUENCIES (ν, cm^{-1}), POTENTIAL ENERGY DISTRIBUTIONS (PED, %) AND PHASE-ANGLE DIFFERENCES [$\Delta\varepsilon$ (OCH_2-CH_2O)]

δ	ν	PED ($\Delta\varepsilon$)	δ	ν	PED ($\Delta\varepsilon$)
	ν_1 (CH_2 as)			ν_2 (CH_2 as)	
0°	2943 A_2	101(180°)	0°	2940 A_1	101(0°)
60°	2943	101(167°)	60°	2940	101(13°)
120°	2943	101(162°)	120°	2940	101(18°)
180°	2942 B_2	101(180°)	180°	2941 B_1	101(0°)
	ν_3 (CH_2 ss)			ν_4 (CH_2 ss)	
0°	2883 A_2	100(180°)	0°	2874 A_1	101(0°)
60°	2883	100(176°)	60°	2874	100(4°)
120°	2883	100(176°)	120°	2873	100(4°)
180°	2883 B_2	100(180°)	180°	2873 B_1	100(0°)
	ν_5 (CH_2 sc)			ν_6 (CH_2 sc)	
0°	1479 A_1	98(0°)	0°	1470 A_2	100(180°)
60°	1478	99(28°)	60°	1470	100(152°)
120°	1475	100(55°)	120°	1471	100(125°)
180°	1473 B_1	100(0°)	180°	1473 B_2	100(180°)
	ν_7 (CH_2 wa)			ν_8 (CH_2 wa)	
0°	1423 A_1	88(0°)	0°	1344 A_2	107(180°)
60°	1415	90(31°)	60°	1347	107(151°)
120°	1395	97(62°)	120°	1356	106(120°)
180°	1373 B_2	106(180°)	180°	1372 B_1	100(0°)
	ν_9 (CH_2 tw)			ν_{10} (CH_2 tw)	
0°	1264 A_2	81(180°)	0°	1252 A_1	81(0°)
60°	1275	76(73°)	60°	1243	85(112°)
120°	1290	73(30°)	120°	1231	89(156°)
180°	1297 B_1	72(0°)	180°	1226 B_2	92(180°)

The ν_7 and ν_8 branches are due to quasi-symmetric ($0°\leq\Delta\varepsilon<80°$) and quasi-antisymmetric ($100°<\Delta\varepsilon\leq180°$) CH_2 wagging modes, respectively, for $\delta=0$—120°. For the ν_7 branch, the C–C stretching mode contributes to PED by 15—20%. The $\nu_7(0)$ vibration was observed as the Raman line at 1398 cm^{-1} while the $\nu_7(\theta)$ vibration was observed as the perpendicular infrared band at 1415 cm^{-1}. Infrared bands due to $\nu_8(0)$ and $\nu_8(\theta)$ were observed at 1345 cm^{-1} (parallel) and 1364 cm^{-1} (perpendicular), respectively.

The ν_9 and ν_{10} branches are due to CH_2 twisting modes. For $\delta=0°$, the $\nu_9(0)$ and $\nu_{10}(0)$ vibrations are antisymmetric and symmetric, respectively, with respect to the local twofold axis. The parallel infrared band at 1244 cm^{-1} is assigned to $\nu_9(0)$. As δ is increased from 0°, however, phase relations of these vibrations are gradually changed and finally are interchanged for $\delta>45°$. Thus the perpendicular bands at 1283 and 1236 cm^{-1} are assigned to $\nu_9(\theta)$ and $\nu_{10}(\theta)$ which are quasi-symmetric and quasi-antisymmetric, respectively.

The ν_{11}—ν_{15} branches in the region 1200—

TABLE 2. CALCULATED FREQUENCIES (ν, cm^{-1}), POTENTIAL ENERGY DISTRIBUTIONS (PED, %) AND PHASE-ANGLE DIFFERENCES[a] ($\Delta\varepsilon$)

	δ	ν	PED ($\Delta\varepsilon$)		
			CH_2 ro	CO st	CCO
ν_{11}	0°	1137 A_1	36(0°)	18(0°)	11(0°)
	60°	1141	32(41°)	28(42°)	13(− 64°)
	120°	1140	26(79°)	42(20°)	19(−118°)
	180°	1130 B_2	18(180°)	60(0°)	26(−180°)
			CO st	CC st	
ν_{12}	0°	1087 A_2	94(180°)	0	
	60°	1098	83(125°)	18	
	120°	1117	81(143°)	21	
	180°	1124 B_1	78(180°)	21	
			CO st	CC st	CH_2 ro
ν_{13}	0°	1073 A_1	47(0°)	46	7(0°)
	60°	1065	46(104°)	26	16(−128°)
	120°	1063	30(100°)	13	43(− 54°)
	180°	1080 B_1	12(180°)	8	60(0°)
			CO st	CC st	CH_2 ro
ν_{14}	0°	964 A_2	10(180°)	0	49(180°)
	60°	949	10(181°)	10	60(96°)
	120°	936	16(172°)	35	26(26°)
	180°	917 B_1	20(180°)	51	16(0°)
			CO st	CH_2 ro	
ν_{15}	0°	866 A_1	50(0°)	46(0°)	
	60°	868	47(5°)	46(92°)	
	120°	836	36(8°)	63(161°)	
	180°	814 B_2	32(0°)	74(180°)	
			CCO	COC	CH_2 ro
ν_{16}	0°	533 A_2	89(180°)	0	33(−180°)
	60°	518	80(150°)	2	30(−155°)
	120°	540	35(146°)	33	11(−154°)
	180°	587 B_2	16(180°)	52	4(−180°)
			CCO	COC	CO to CC to
ν_{17}	0°	274 A_1	24(0°)	17	16(0°) 19
	60°	322	16(32°)	46	6(44°) 6
	120°	365	57(74°)	29	9(− 23°) 4
	180°	316 B_1	100(0°)	0	10(−180°) 4
			CCO	COC	CO to CC to
ν_{18}	0°	218 A_1	6(0°)	48	22(0°) 11
	60°	221	25(55°)	21	23(34°) 27
	120°	224	60(63°)	16	5(−174°) 17
	180°	289 B_2	44(180°)	30	16(0°) 0
			CO to	CC to	
ν_{19}	0°	105 A_2	90(180°)	0	
	60°	123	65(161°)	22	
	120°	179	31(−150°)	58	
	180°	196 B_1	20(−180°)	78	
			CCO	CO to	
ν_{20}	0°	0 A_1	—	—	
	60°	72	54(11°)	38(45°)	
	120°	86	14(− 35°)	82(69°)	
	180°	38 B_2	10(−180°)	80(0°)	
			CO to	CC to	
ν_{21}	0°	0 A_1	—	—	
	60°	9	56(73°)	36	
	120°	2	67(94°)	19	
	180°	37 B_1	64(180°)	13	

a) Phase-angle differences $\Delta\varepsilon(OCH_2\text{–}CH_2O)$ are shown for CH_2 ro and CCO, while $\Delta\varepsilon$(C–O–C) are shown for CO st and CO to.

800 cm^{-1} are associated with C–O and C–C stretching modes and CH_2 rocking modes (Table 2, Fig. 1). Vibrational coupling among these modes is also shown in Fig. 3.

The ν_{11} and ν_{15} branches arise from vibrational coupling of CH_2 rocking modes and quasi-symmetric C–O stretching modes, although relative contributions of these modes vary with phase difference (Fig. 3). Also phase relations ($\Delta\varepsilon$) of rocking modes of CH_2–CH_2 groups vary with phase difference (δ), from $\Delta\varepsilon=0°$ for $\delta=0°$ to $\Delta\varepsilon=180°$ for $\delta=180°$. The Raman lines at 1126 and 861 cm^{-1} are assigned to $\nu_{11}(0)$ and $\nu_{15}(0)$ and the perpendicular infrared bands at 1149 and 844 cm^{-1} are assigned to $\nu_{11}(\theta)$ and $\nu_{15}(\theta)$, respectively.

The ν_{12} branch around 1100 cm^{-1} is primarily associated with the C–O–C antisymmetric stretching mode ($125°\leq\Delta\varepsilon\leq180°$), in accord with empirical assignments of strong bands around 1100 cm^{-1}. The very strong parallel band at 1102 cm^{-1} and strong perpendicular band at 1119 cm^{-1} are assigned to $\nu_{12}(0)$ and $\nu_{12}(\theta)$, respectively. C–C stretching modes contribute about 20% of PED for $\delta>60°$ (Fig. 3).

The ν_{13} and ν_{14} branches are associated with C–O and C–C stretching modes and CH_2 rocking modes. Frequencies of the ν_{13} branch do not vary much with phase difference (δ), but the nature of ν_{13} vibrations changes markedly with δ. For $\delta=0°$, the $\nu_{13}(0)$ vibration is due to the C–O–C symmetric stretching mode ($\Delta\varepsilon=0°$) and C–C stretching mode. As δ is increased, however, PED contributions of these modes decrease and instead PED of CH_2 rocking modes increases up to 60% for $\delta=180°$ (Fig. 3). The perpendicular infrared band at 1062 cm^{-1} is assigned to $\nu_{13}(\theta)$.

The $\nu_{14}(0)$ vibration is primarily associated with the CH_2 rocking mode ($\Delta\varepsilon=180°$), giving rise to the parallel infrared band at 963 cm^{-1}. As phase difference is increased, PED contribution of C–C stretching modes increases, and for $\delta=\theta$ the $\nu_{14}(\theta)$ vibration is due to the coupling of the quasi-symmetric CH_2 rocking mode and C–C stretching mode, giving rise to the perpendicular band at 947 cm^{-1}.

Low Frequency Branches

In the region below 600 cm^{-1}, there are six vibrational branches, ν_{16}—ν_{21}, as shown in Fig. 2. These branches are associated with C–C–O and C–O–C bending modes and C–O and C–C internal-rotation modes (Table 2 and Fig. 4).

The $\nu_{16}(0)$ vibration is primarily associated with the antisymmetric C–C–O bending mode, giving rise to the parallel band at 529 cm^{-1} with a weak component at 508 cm^{-1}. The doublet splitting is due to Fermi resonance.[5] Because of appreciable contribution of the CH_2 rocking mode (33% of PED), this infrared band is shifted to 444 cm^{-1} (doublet) for perdeuterated species $(-CD_2CD_2O-)_p$. As phase difference is increased, PED contributions of quasi-antisymmetric C–C–O bending mode and quasi-antisymmetric CH_2 rocking mode are gradually replaced with PED of the C–O–C bending mode (Fig. 4). For $\delta=\theta$, the $\nu_{16}(\theta)$ vibration gives rise to the Raman line at 537 cm^{-1}.

The Raman line at 279 cm^{-1} is due to the $\nu_{17}(0)$ vibration of the A_1 species, a coupled vibration of the C–C–O and C–O–C bending modes and C–O and C–C internal-rotation modes (Fig. 4). As δ is increased, PED changes remarkably until finally, for $\delta=180°$, PED is essentially associated with the symmetric C–C–O bending mode. For $\delta=\theta$, $\nu_{17}(\theta)$ is a coupled vibration of the quasi-symmetric C–C–O bending mode and C–O–C bending mode, giving rise to the infrared band and Raman line at 363 cm^{-1}.

The Raman line at 216 cm^{-1} is due to the $\nu_{18}(0)$ vibration, a heavily coupled vibration of bending and internal-rotation modes (Fig. 4). Again PED contributions of the four modes vary markedly with phase difference. The $\nu_{18}(\theta)$ vibration gives rise to the perpendicular infrared band at 216 cm^{-1}.

The parallel far-infrared band at 107 cm^{-1} is due to the $\nu_{19}(0)$ vibration, associated with the antisymmetric internal-rotation mode of C–O bonds. However, as δ is increased, PED contribution of the C–O internal-rotation mode is gradually replaced with PED of the C–C internal-rotation mode (Fig. 4). The $\nu_{19}(\theta)$ vibration gives rise to the perpendicular infrared band at 165 cm^{-1}.

Acoustic Branches

The lowest-frequency branches, ν_{20} and ν_{21}, are the acoustic branches of polyethylene-glycol chain. The non-genuine vibrations $\nu_{20}(0)$ and $\nu_{21}(0)$ correspond to the translation (along the axis) and rotation (about the axis). For $\delta\sim0°$, the longitudinal stretching mode and twisting mode of the chain are coupled to yield the ν_{20} (coupling ratio of 3 : −2) and ν_{21} (ratio of 2 : 3) vibrations.*3 Potential energies of these vibrations are associated largely with quasi-symmetric C–C–O bending mode and with internal-rotation modes of C–C and C–O bonds (quasi-symmetric), respectively.

For $\delta=\theta$, the ν_{21} vibration is reduced to a non-genuine vibration corresponding to the translational mode perpendicular to the chain axis. For $\delta\sim\theta$, the ν_{21} vibration is the bending vibration of the molecular chain. The potential energy of this bending vibration is largely associated with internal-rotation modes of C–O bonds.

Frequency Distribution

For analyses of neutron-scattering peaks, in the present study, the frequency distribution of chain vibrations was calculated from dispersion curves of the twenty-one branches of polyethylene glycol (Figs. 1 and 2). The phase-difference region of $0°\leq\delta\leq180°$ was equally divided into 1800 subsections, and representative phase differences were taken as 0.05°, 0.15°,⋯, 179.85° and 179.95°, for which vibrational frequencies of each branch were calculated.

For the phase-difference region of $0°\leq\delta\leq15°$, vibrational frequencies of the optical branches (ν_1—ν_{19}) were calculated with even functions,

$$\nu(\delta)=\nu(0°)+a_2\delta^2+a_4\delta^4 \quad (1)$$

which satisfy frequencies previously calculated for $\delta=0°$, 15° and 30°, whereas frequencies of the acoustic branches (ν_{20} and ν_{21}) were calculated with odd functions,

$$\nu(\delta)=a_1\delta+a_3\delta^3 \quad (2)$$

which satisfy frequencies for $\delta=0°$, 15° and 30°.

An intermediate phase-difference region was divided into sub-regions of 15—30°, 30—45°,⋯, 135—150°, and 150—165°. For each sub-region of $\delta_0\leq\delta\leq\delta_0+15°$, vibrational frequencies were calculated with the following equation,

$$\nu(\delta)=\nu(\delta_0)+b_1(\delta-\delta_0)+b_2(\delta-\delta_0)^2+b_3(\delta-\delta_0)^3 \quad (3)$$

which satisfies frequencies for $\delta=\delta_0-15°$, δ_0, $\delta_0+15°$ and $\delta_0+30°$.

Finally, for the phase-difference region of $165°\leq\delta\leq180°$, vibrational frequencies were calculated with even functions,

$$\nu(\delta)=\nu(180°)+c_2(180°-\delta)^2+c_4(180°-\delta)^4 \quad (4)$$

which satisfy frequencies for $\delta=150°$, 165° and 180°.

*3 For the polyethylene-glycol chain in the right-handed 7_2 helix, the stretching mode of the chain is accompanied with rotation of the twisting mode in the left-handed and right-handed sense, respectively, for the ν_{20} and ν_{21} vibrations for $\delta\sim0°$.

After vibrational frequencies were calculated for all the branches, the number of vibrations was counted in the frequency sections of 10 cm^{-1} for high-frequency branches ($>700\ cm^{-1}$) and of 5 cm^{-1} for low-frequency branches ($<700\ cm^{-1}$). The frequency-distribution histograms thus obtained are shown in Figs. 1 and 2, together with dispersion curves.

Neutron Scattering Peaks

Thermal-neutron scattering of polyethylene glycol was measured by Trevino and Boutin[3] and inelastic-scattering peaks were observed at 535, 380—310 and 228 cm^{-1} in the frequency region of 600—200 cm^{-1}.*4 Vibrational assignments of these peaks will be made with reference to frequency distribution peaks (and PED) calculated in the present study.

The observed scattering peak at 535 cm^{-1} corresponds to the distribution peaks at 530 and 515 cm^{-1}. These distribution peaks arise from the ν_{16} vibrations for $0° \leq \delta \lesssim 110°$ and are largely associated with quasi-antisymmetric C–C–O bending mode. Another distribution peak at 585 cm^{-1} (C–O–C bending) was not resolved in the neutron-scattering measurement.

The broad scattering peak around 380—280 cm^{-1} corresponds to the distribution peaks at 370, 315 and 280 cm^{-1}. The peak at 370 cm^{-1} arises from the maximum portion of the ν_{17} branch for $\delta = 90$—$120°$. As shown in Fig. 4, these ν_{17} vibrations are associated with C–O–C bending and quasi-symmetric C–C–O bending modes. On the other hand, the peak at 315 cm^{-1} arises from the ν_{17} vibrations for $\delta \sim 180°$, and accordingly is due to quasi-symmetric C–C–O bending mode. The distribution peak at 280 cm^{-1} arises from ν_{17} vibrations for $\delta \sim 0°$ and ν_{18} vibrations for $\delta \sim 180°$.

The high distribution peak at 220 cm^{-1} arises from the flat portion of the ν_{18} branch, where vibrational frequencies hardly vary for phase differences of $0° \leq \delta \lesssim 120°$ (Fig. 2). In fact, a strong scattering peak was observed at 228 cm^{-1}. These ν_{18} vibrations are coupled vibrations of C–O–C and C–C–O bending modes and C–C and C–O internal-rotation modes.

Thus, neutron-inelastic scattering peaks in the region 600—200 cm^{-1} were assigned, with reference to the frequency distribution calculated for an isolated single chain of polyethylene glycol. However, in the region below 200 cm^{-1}, interchain interactions become significant, so that observed scattering peaks may not be compared with the distribution peaks of an isolated chain. For more realistic analyses of neutron scattering in the low-frequency region, treatments of crystal vibrations are required. Nevertheless, inelastic scattering peaks were observed at 120 and 80 cm^{-1}, apparently corresponding to the Raman lines at 126 and 75 cm^{-1}.[12]

Conclusion

The infrared absorption, Raman scattering, and neutron inelastic scattering spectra of polyethylene glycol were analyzed, on the basis of dispersion curves, frequency distribution and potential-energy distributions calculated for an isolated chain. The dispersion curves are also useful for vibrational analyses of infrared and Raman spectra of model oligomers and for treating heat capacities due to optical branches. The present study was reported, in more detail, in a thesis by Matsuura.[13]

Numerical calculations of the present study were carried out with a HITAC 5020E computer at the University of Tokyo and a NEAC 2200-500 computer at Osaka University.

*4 In the region above 600 cm^{-1}, a scattering peak was observed at 868 cm^{-1}.[3] This scattering peak corresponds to the distribution peak at 870 cm^{-1} (Fig. 1), which is associated with C–O stretching and CH_2 rocking modes.

12) R. F. Schaufele, *Trans. New York Acad. Sci.*, to be published.

13) H. Matsuura, "Vibrational Spectra of Polyethylene Glycol and Related Molecules," Thesis, Chapter II, Osaka University, 1968.